Research Article Vol. 38, No. 12 / December 2021 / Journal of the Optical Society of America B 3639

Journal of the Optical Society of America B

OPTICAL PHYSICS

Forward terahertz wave generation from liquid gallium in the non-relativistic regime

Kareem Garriga Francis,[1,†] Yuqi Cao,[1,2,†] Yiwen E,[1] Fang Ling,[1,3] Mervin Lim Pac Chong,[1] and Xi-Cheng Zhang[1,*]

[1]The Institute of Optics, University of Rochester, Rochester, New York 14627, USA
[2]College of Control Science and Engineering, Zhejiang University, Hangzhou 310027, China
[3]College of Electronics and Information Engineering, Sichuan University, Chengdu 610064, China
*Corresponding author: xi-cheng.zhang@rochester.edu

Received 2 July 2021; revised 5 October 2021; accepted 17 October 2021; posted 18 October 2021 (Doc. ID 435759); published 15 November 2021

We characterize a terahertz (THz) source based on plasma in liquid gallium. The dependence of the emitted THz pulse energy on second-order phase, pump pulse energy, and polarization of the short laser pulse is demonstrated. Our study suggests that the THz emission mechanism is due to the ponderomotive force and is aided by a direct-field driven term. The proposed source and accompanying generation mechanism are studied under a non-relativistic regime ($10^{15} < I < 10^{18}$ W/cm^2) for forward directed THz under a single pump excitation scheme.

https://doi.org/10.1364/JOSAB.435759

The generation of THz waves from metal surfaces under ultrashort pulse excitation is a topic that has been studied extensively. In the relativistic regime ($I > 10^{18}$ W/cm^2), metals have been shown to provide THz pulse energies in excess of 50 mJ via coherent transition radiation (CTR) from thin metal foils [1]. Further, high THz peak electric field was also generated from metals in excess of 0.9 GV/cm via gyrotron-like electron emission [2]. This high-peak field process was kick-started by femtosecond laser ionization on a metal wire tip. In the relativistic regime, the material ionization threshold is greatly surpassed since the laser peak focal electric field strength reaches or surpasses the inter-atomic field strength, and the net displacement of electrons is no longer zero. Although large-scale laser facilities are typically required to observe these mechanisms, they show that metals have an abundant potential when it comes to developing the most intense THz sources.

Metals have also been investigated as THz sources under weak ($I < 10^{14}$ W/cm^2) pump pulse excitation. In this regime, three possible generation mechanisms used to explain the results, including surface optical rectification (OR) [3–5], nonlinear current generation [6–8], and thermal gradients [9,10]. In these studies, the THz generation is characteristically limited to 1 nJ in energy and shows a clear preference for p-polarized incident fields at 800 nm. Interestingly, the experiments show that there is often a preference for thicknesses larger than the metal effective absorption depth. A fully consistent explanation for this phenomenon is not yet available. Most notably, in the weak pump regime, the laser-induced plasma is not required, showing that the generation mechanism dramatically switches between the relativistic and weak pump pulse excitation schemes.

Understanding the full picture of the mechanism regimes for metals will be key to fully exploiting their advantages to develop the most efficient THz sources. Nevertheless, to the best of our knowledge, no studies have been reported for forward (detected along the z axis) THz wave generation from liquid metals in the non-relativistic ionizing regime ($10^{15} < I < 10^{18}$ W/cm^2) under single pump configuration. This regime is critically different from those where CTR is enacted because the ponderomotive acceleration enacted is not enough to ballistically propel electrons through the targets. Further, the laser cannot lead to a net displacement of the electrons.

In this study, we characterize a THz source based on a liquid metal jet with a peak field of 0.6 kV/cm under single-color and single-pump excitation. To avoid the issue of target ablation and material damage changing data on a shot-by-shot basis, a flowing liquid metal jet is used rather than a solid metal target. Due to our experimental configuration and single-pump excitation scheme, our studies are fundamentally different in terms of the physical mechanism from reference [11], where forward radiation in the double-pump geometry was studied. In fact, the interest in pursuing this source is the fact that under the single-pump regime, the high absorption and reflection from metals at both optical and THz frequencies would lead us to assume that no THz generated could be detected in the forward direction. Furthermore, in presenting our study, we grow one step closer toward completely characterizing metal THz sources to fully understand their generation regimes.

The experimental system for THz wave generation via liquid metal utilizes a commercial Ti:sapphire laser amplifier with a center wavelength of 800 nm, 1 kHz repetition rate, and 43 fs transform-limited pulses. In our experiments, this corresponds to an intensity regime of $10^{15} - 10^{16}\,\mathrm{W/cm^2}$ when using a 50 mm focal length lens. Up to a second-order phase of $+12600\,\mathrm{fs^2}$ and $-12600\,\mathrm{fs^2}$ is applied to the pulse corresponding to an 800 fs temporal broadening via negative and positive chirping, respectively. We choose to primarily describe broadening in terms of a second-order phase to eliminate any ambiguity in the dispersion profile. The experimental geometry is shown in Fig. 1(a).

Optical pulse duration is measured with a second-harmonic generation (SHG) interferometric autocorrelator. The diameter of the optical beam is 13 mm, and the laser pulses are focused onto a 210 μm liquid gallium (LG) jet with a 50.8 mm focal length lens. Under this configuration, and in the absence of photoionization effects, the large optical and THz absorption coefficients prevent any significant propagation or output coupling of optical and THz waves. We choose LG as the target due to its attractive physical properties compared to other low-melting-point metals as noted in our previous publication [12]. The flow rate of the LG jet is controlled at 3.8 m/s steadily to ensure that each pump laser pulse interacts with a fresh target. An $x - z$ translation stage is applied to control the position of the LG jet about the laser focus. The LG jet can be translated along the x axis for fine adjustment of the effective thickness and incidence angle $\alpha = \arcsin^{-1}(\Delta x/R)$ measured from the surface normal where Δx is the shift in the x axis from the center and R is the jet radius [13].

The peak THz electric field strength is measured via standard electro-optical sampling with 3 mm ZnTe once the source is optimized. More details about the experimental setup can be found in our previous work [12]. Since the p-polarized pump pulse is more efficient in LG case, all the data shown hereafter are under the excitation of p-polarized pump pulses unless otherwise indicated. The pump pulse is temporally chirped to maximize the THz signal.

The THz signals excited from single color laser pulse in air and LG jet are shown in Fig. 1(b). Compared to the maximum signal generated by an air-plasma source with 370 fs pulse duration, the LG source has a higher energy and peak field strength with a maximum optical-to-THz energy conversion efficiency of 2.5×10^{-7}. It should be noted that for the bandwidth represented in this figure, the measurements were made with 3 mm

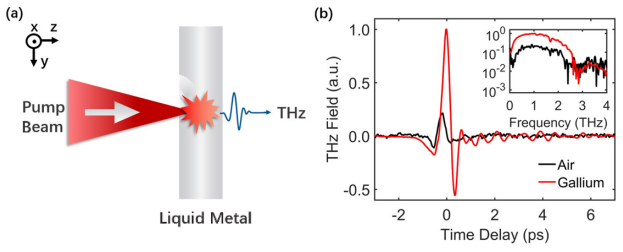

Fig. 1. (a) Focusing geometry of the experimental setup as seen on the $y - z$ plane (side view). The liquid metal flows along the y direction, and THz is collected in the forward (z) direction. (b) THz waveforms generated from air plasma and LG jet, respectively. The corresponding comparison in the frequency domain is shown in the inset.

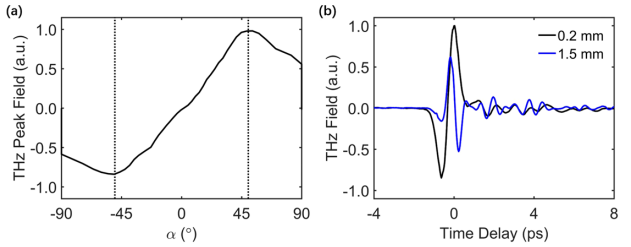

Fig. 2. (a) Normalized THz field strength as a function of the incident angle from the LG jet. The dashed black line represents the maximum angle of THz fields for LG. The area between these two lines stands for moving the jet from one side to the other side. (b) THz waveforms generated from LG lines with two different needle diameters, which are 0.2 and 1.5 mm.

ZnTe and are thus band limited by the EO crystal. Additionally, the system was optimized for LG generation and is not representative to the best case of air-plasma generation where the bandwidth is known to be much larger. As seen in Fig. 2(a), translation of the jet along the x axis and keeping the detection static shows two nearly identical peaks corresponding to angles that are opposite in sign. The z position is optimized before each measurement. We note that the x axis is perpendicular to the optical pulse propagation direction. The optimum incidence angles are $\pm 54°$ considering a displacement along x of 85 μm. Since the jet maintains a cylindrical symmetry, we initially considered that electron circulation in the Ga could explain the radiation of THz waves. In this scheme, the femtosecond (fs) laser pulse causes the electrons to move tangentially about the jet akin to a loop antenna. However, the expectation of this radiation pattern would be isotropic onto 4π space regardless of incidence onto the jet. The curve in Fig. 2(a) shows two peaks with reversed polarity, which is caused by the flipped dipole for the opposite incident angle. This observation is a strong argument for the application of the dipole model and rejection of current circulation effects as argued in [12,13]. Moreover, the explored intensity regime is far too low to produce any significant forces capable of trapping electrons in a circulation motion (i.e., the effects of the magnetic field are not strong enough).

In translating the pump near the edge of the LG jet, the THz yield is a coherent combination of radiation from the LG and air plasmas. Outside of the LG jet, the signal drastically reduces to the level of the air-plasma source evaluated under the same experimental conditions. In the LG case, the absorption at both optical and THz frequencies does not allow for significant propagation within the material. Because of this, we believe that the plasma is formed at the jet surface. The fact that the THz waves do not propagate within the jet is confirmed by absence of a large THz peak field position change when the x axis is shifted or when the LG jet is turned off, given that the LG refractive index at THz > 100 [11]. This is also strong evidence that the generation is from a single plasma current as opposed to a front and back surface. To explain this observation, we initially believed that the Ga target could be compressed or pushed away from the laser focal area by a strong ponderomotive force induced by the fs laser. However, later experiments with a 1.5 mm LG jet diameter showed a similar signal as that of 0.2 mm as can be seen in Fig. 2(b). Because a relatively strong signal can still be seen when the laser intensity is $10^{15}\,\mathrm{W/cm^2}$,

we can conclude that no significant compression can occur to explain the unmitigated propagation of THz from the plasma–metal boundary. A secondary metric we use to reach this conclusion is the fact that when needle diameters above 1 mm are used, strong THz waves can still be detected even at zero-degree incidence. At zero incidence onto a 1.3 mm jet, a THz wave can still be produced. The plot in Fig. 3 shows the THz waveform produced by a 1.3 mm LG jet at zero-degree incidence compared to the signal produced along the optimized angle for this diameter. Although the signal is weak (we find a 100 times decrease relative to when the position/angle of the LG jet is optimized), the expectation is that the absorption of THz through the remaining unionized Ga would stop the THz propagation altogether. Additionally, a nonrelativistic laser cannot compress a millimeter (mm) target below the skin depth to allow for THz wave propagation. We would like to note that the shift seen in Fig. 3 is not due to propagation through Ga. Considering the index of refraction of Ga and the thickness of the material, it is easy to see that this is the case. Instead, we believe the shift is due to two parameters: changes in the diffraction of the Ga around the remaining jet and changes due to alignment errors in setting up the LG jet between the two scans. As mentioned in our manuscript, we believe that the THz results from a current oscillation due to nonlinear effects at the surface of the Ga. The transients radiated from this current must diffract around the remaining Ga material to the detector. Additionally, laser focus onto the Ga encourages fast oxidation, which causes the needle to become clogged very often. In changing the needle, it is easy to misalign the system and introduce artificial delays.

Furthermore, because Ga is not optically transparent, the plasma ionization cannot cascade and fully ionize the channel. It should be noted that when setting up the experiment, nearly no optical beam can be seen to transmit through the jet after the plasma if evaluated at 0° incidence excluding a portion that diffracts around the jet.

We hereby consider a hydrodynamic approach in describing the radiation from the jet plasma. It is assumed that, along the center of the jet, although there is a contribution due to many angles when the focused beam's waist is considered, the difference in the angles is small enough to consider the problem as a zero-incidence model. The ionization action does indeed compress the jet, but the compression factor caused by the plasma shock wave at non-relativistic intensity is considered small. As such, a larger THz yield is expected since the pump pulse can more efficiently further ionize the material, but it should be stated that the material cannot be fully ionized in our non-relativistic intensity regime. Learning from experiments done

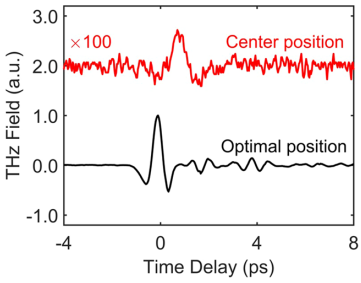

Fig. 3. THz waveforms detected for a 1.3 mm LG jet at the optimal angle of 67° and at zero-degree incidence.

in weak and high intensity regimes, we expect that an optimum thickness exists related to the ionization events. In this region, it is expected that interference effects lead to an overall reduction in the THz yield due to the plasma asymmetric gradient and diffraction. We can theoretically describe the emission of THz waves from a filament spark at the material boundary by starting with the electron hydrodynamic equation. The model expands on the work presented in references [14,15] and is applied to condensed media to determine a current density whose oscillation is proportional to the radiated THz waves. Strong laser ionization at the surface of the jet directly leads to a complex electron density gradient due to concurrent ionization of air. The THz wave produced in this manner is radiated within the first few picoseconds (ps) of the plasma lifetime and cannot be described as propagating through a channel ionized through the material. We can also assume that the optical beam cannot "push" Ga away to allow for THz wave propagation. This is because the laser ponderomotive energy needed to displace Ga away from the propagation direction would be unphysical, as the unionized Ga would need to be displaced at speeds much greater than the speed of sound as evaluated through the general equation for kinetic energy.

Instead, we surmise that the radiation produced at the plasma–metal boundary diffracts about the jet and onto our detector. In this model, the translation of the jet leads to the emergence of photocurrent-like excitation. Within the parameters of our model, our investigations indicate that the strongest signal is retrieved when the contribution of the ponderomotive force and the field-driven term can be significantly mixed to produce a seemingly asymmetric transverse plasma current akin to the two-color generation process in air. The result is a fully consistent and all-encompassing model that can be used to describe generation schemes regardless of the material so long as a plasma is enacted onto it. In the simplest case, the model can be made using a zero-incidence excitation to simultaneously describe the air in a single-color and two-color regime. To apply this model to the LG line, we simply rotate the axes of interaction to account for the oblique incidences achievable with the present air–material boundaries.

Taking an optical pulse to be polarized in the x direction and traveling along z, the electron equation of motion describing the dynamics of matter influenced by an optical pulse is

$$\frac{\partial \vec{v}}{\partial t} + \left(\vec{v}\cdot\nabla\right)\vec{v} + 2\gamma\,\vec{v} = -\frac{e}{m}\left(\vec{E} + \eta\vec{v}\times\vec{B}\right). \quad \textbf{(1)}$$

Above, $\vec{v}$ is the unperturbed electron velocity, γ is the damping factor, e is the electron charge, m is the electron mass, $\vec{E}$ is the electric field, $\vec{B}$ is the magnetic flux, and η is a perturbation constant. We hold that although the electrons move and the plasma is treated as a fluid, the ions are relatively inert, so that the electron continuity equation is given as

$$\frac{\partial N_e(x,\,z,\tau_R)}{\partial t} + \nabla\cdot N_e(x,\,z,\tau_R)\vec{v} = N_{at}\,W(\omega_o,\,I)$$

$$-\beta_{\text{recomb}}N_e^2(x,\,z,\tau_R) - \beta_{\text{attach}}N_e(x,\,z,\tau_R)N_{at}^2, \quad \textbf{(2)}$$

where $N_e(\mathrm{x},\,\mathrm{z},\tau_R)$ is the electron density, N_{at} is the metal atomic density, and W is the ionization rate. However, because

of the complex plasma gradient, the electron density is a sensitive function of both position (x and z) and time (taken in the frame of reference of the pulse via $\tau_R = t - z/v_g$).

When a strong laser pulse interacts with a material and ionization occurs, there are many factors to consider. Of importance to us is the dominant photoionization process. Due to their number densities, materials are limited in their response to shock waves by the free-electron mean-free time (a parameter denoting the average time between collisions). This time is different for all materials and can range between sub-fs to ps time scales. As an example, in plasma formed in condensed media, the mean-free time is on the order of 0.1–1 fs compared to >300 fs in gas media [16]. The pulses we use are typically over 100 fs, and the optical breakdown threshold tends to be on the order of inverse pulse duration in watts per squared centimeter (W/cm^2). This means that more than enough time along the pulse evolution exists to efficiently enact cascade ionization. In our case, there are a few cycles of the pulse available for breakdown via cascade ionization prior to filamentation or self-focusing being achieved. In order for cascade ionization to have an impactful contribution (regardless of whether tunnel or multiphoton kick-started ionization), the pulse duration of the laser must be very long compared to the mean-free time of electrons. Therefore, we believe cascade is dominant over tunnel ionization—the mean-free time is nearly 1 fs, but the pulse durations we use to optimize the THz conversion efficiency are hundreds of fs. Although we believe that tunnel ionization kick-starts the plasma, we believe cascade ionization dominates the ionization process due to the longer pulse duration contrasted to the mean-free time of the electrons in the LG as compared to air. As such, the rate function is modelled as intensity dependent. The extra terms refer to the recombination and attachment coefficients. However, because the plasma lifetime is so long compared to the pulse, these can usually be neglected—especially in an evaluation of the transient regime. A simplification $\vec{E_F}(t) = \hat{x}E_x + \hat{z}E_z$ is taken to describe the electromagnetic field producing the plasma filament. The problem is treated semiclassically, as the plasma is not a quantum plasma, and a perturbation of the continuity equation and an evaluation based on Gauss's law from Maxwell's equations yields

$$\nabla \cdot \frac{\partial \vec{E_F^{(0)}}}{\partial t} \approx -\frac{e}{\varepsilon_o}\left[N_{at} W\left(\omega_o, \vec{E}\right) - \nabla \cdot N_e^{(0)} \vec{v^{(0)}}\right] \quad (3)$$

and

$$\frac{\partial \vec{E_F^{(1)}}}{\partial t} \approx \frac{e}{\varepsilon_o}\left(N_e^{(0)} \vec{v^{(1)}} + N_e^{(1)} \vec{v^{(0)}} + N_e^{(1)} \vec{v^{(1)}}\right). \quad (4)$$

Using a perturbation equation solution similar to Ref. [14] and a rotation provided $x' = x\cos\theta + z\sin\theta$ and $z' = -x\sin\theta + z\cos\theta$, $\vec{v} = \hat{x}v_x' + \eta\hat{z}v_z'$. The equation of motion is also perturbed, and the magnetic field component is simplified via Laplace transform. The primed values signify that a coordinate rotation $v_z' = v_z\cos(\alpha) + v_x\sin(\alpha)$ and $v_x' = -v_z\sin(\alpha) + v_x\cos(\alpha)$ has been enacted to produce

$$\frac{\partial v_x'}{\partial \tau_R} + \gamma v_x' = \frac{-e E_x'(\tau_R)}{m} \quad (5)$$

and

$$\frac{\partial v_z'}{\partial \tau_R} + \gamma v_z' = \frac{1}{2v_g}\frac{\partial}{\partial \tau_R}\left|v_x'\right|^2 + \frac{\gamma}{v_g}\left|v_x'\right|^2 - \frac{e}{m}E_z'(\tau_R). \quad (6)$$

Above, the spatial derivatives have been converted to temporal derivatives by noting that $v_x' = v_x'(x, \tau_R)$, so $\frac{\partial v_x'}{\partial z} = \frac{\partial v_x'}{\partial \tau_R}\frac{\partial \tau_R}{\partial z} = -\frac{1}{v_g}\frac{\partial v_x'}{\partial \tau_R}$. If we take the laser intensity to be represented as $I(\tau_R) = \varepsilon_o v_g n(\omega_o)|\vec{E_F}(\tau_R)|^2/2$, and the laser central frequency as ω_o, the variance of the electron motion along the transverse (x axis) plane is given by the expression $\langle v_x^{2'}(\tau_R)\rangle = e^2 I' x(\tau_R)/[v_g\varepsilon_o n(\omega_o)m^2(\gamma^2 + \omega_o^2)]$. In the absence of a quantum plasma, the electron longitudinal motion that can be written as

$$\frac{\partial v_z'}{\partial t} + \gamma v_z' = \frac{e^2}{2v_g\varepsilon_o n(\omega_o)m^2\left(\gamma^2 + \omega_o^2\right)} \times \left[\frac{1}{v_g}\frac{\partial I_x'(\tau_R)}{\partial \tau_R} + \frac{2\gamma I_x'(\tau_R)}{v_g}\right] - \frac{e}{m}E_z'(\tau_R). \quad (7)$$

The first term on the right-hand side indicates the temporal version of the ponderomotive force. The second term is related to the radiation pressure. The last term is a direct field-driven term. The primed terms indicate that a rotation has been enacted due to the TM wave and variation in angle of incidence α. We consider small perturbations in the plasma density and assume that the electron velocity must be well below the group velocity since the group velocity is nearly at the speed of light. As such, $v^{(1)}/v_g = v_{z'}/v_g \approx 0$. Reevaluating the continuity equation and noting that for the relatively inert ions $N_i \approx N_e^{(0)}$, we reach the plasma field equation

$$\frac{\partial^2 E_{pl'}}{\partial \tau_R^2} + \gamma\frac{\partial E_{pl}'}{\partial \tau_R} + \omega_p'^2 E_{pl}' = \frac{e\omega_p'^2}{2v_g^2\varepsilon_o n(\omega_o)m^2(\gamma^2 + \omega_o^2 t)}\left[\frac{\partial I_x'(\tau_R)}{\partial \tau_R} + 2\gamma I_x'(\tau_R)\right] - \omega_p'^2 E_z'(\tau_R). \quad (8)$$

The quantity $e^2 N_e^{(0)}/m\varepsilon_o$ is the squared plasma frequency ω_p, $\omega_p' = \omega_p/n(\omega_o)'$, and $\varepsilon = \varepsilon_o\varepsilon_R = n^2(\omega_o)\varepsilon_o$. To solve for the field induced by the plasma wave, we use the Fourier transform method. We can take the laser intensity to have a formalism $I(\omega) = I_o\int_0^{\tau_p} e^{-(\frac{\tau_R}{T_O})^2(1+jC)}e^{-j\omega\tau_R}d\tau_R$. In the single-color and single-pump limit, the rotated longitudinal current is described after the transform operation as

$$J_z'(\tau_R) = -e N_e(\mathrm{x}, \mathrm{z}, \tau_R)v_z'. \quad (9)$$

The spectrum is given as $J_z'(\omega) = j\omega\varepsilon E_{pl}'(\omega)$. In the single-color and single-pump limit, the rotated longitudinal current is described after the transform operation as

$$J_z'(\omega_{\mathrm{THz}}) = \frac{e\omega_p^2\cos^2(\alpha)}{2v_g^2 n(\omega_o)m^2(\gamma^2+\omega_o^2)} \cdot \frac{2j\gamma+\omega_{\mathrm{THz}}}{\omega_{\mathrm{THz}}^2-\omega_p'^2+j\gamma\omega_{\mathrm{THz}}} \cdot I_o e^{\frac{-\omega_{\mathrm{THz}}^2 T_o^2}{1+jC}} + \frac{j\omega_{\mathrm{THz}}\varepsilon_o\omega_p^2 E_o e^{\frac{-\omega_{\mathrm{THz}}^2 T_o^2}{2(1+jC)}}}{\omega_p'^2-\omega_{\mathrm{THz}}^2-j\gamma\omega_{\mathrm{THz}}}\sin(\alpha). \quad (10)$$

As for the transverse component, the change in the density of electrons is given by $dN_e(\tau_R)$ and $\frac{\partial J_x'(\tau_R)}{\partial \tau_R} = -e\frac{\partial N_e(\tau_R)}{\partial(\tau_R)}v_{d,x}'(\tau_R)$, where we can also model $v_{d,x}'(\tau_R) = \frac{eE'x(\omega)}{m_e}\frac{\sin(\omega\tau_R)}{\omega}$ as the electron drift velocity. The change in the electron density is supplied by the rate function, and the THz field can be found by the relation $E_{\mathrm{THz}} \propto \frac{\partial J_x'(\tau_R)}{\partial \tau_R} = -e\frac{\partial N_e(\tau_R)}{\partial \tau_R}v_{d,x}'(\tau_R) \propto W(\omega, I)v_{d,x}(\tau_R)$. Unfortunately, we cannot yield a proper estimate for parameters such as the electron number density to properly model the THz field.

In the above example and under the single-color limitation, the drift velocity is an odd function with respect to temporal grid. The ionization rate is a nearly even function in the case of tunneling ionization, but not in the case of cascade ionization. As such, the product of the cascade ionization rate and the drift velocity is odd, and we get a nearly net zero current [17]. This means that the x' contribution (transverse current) is effectively zero. This can also be further shown by conducting the experiment under a two-color excitation scheme as is typically done with other laser-plasma sources. To produce a two-color field, we use a β-barium borate (BBO) crystal in a second-harmonic generation scheme as the optical beam focuses onto the LG target. It is critical to note that even when a BBO is used in our system, there is no change to the THz peak field or energy as is typically expected. This reinforces our observation that cascade ionization dominates, as the rate function for cascade ionization would not lead to a net transverse current enhancement according to the photocurrent model. Performing one final rotation back to $x-z$, the current densities are $J_z(\omega) \approx J_z'(\omega)\cos(\alpha)$ and $J_x(\omega) \approx J_z'(\omega)\sin(\alpha)$. At very large angles, the current is nearly completely tangential, and a larger THz reflected signal is expected. On zero incidence, the current is completely longitudinal. In the case of middle angles (30°–70°) the source has an asymmetric contribution like the two-color generation case. As such, the photocurrent model is seemingly applicable. However, the similarity to the photocurrent model is only in terms of its form. The photoionization effects are not as significant in determining the transverse expression. Instead, the transverse current becomes dominant when the field-driven term has more weight.

As seen in Fig. 4(a), the maximum THz yield is observed for a second-order phase $\pm 4700\,\mathrm{fs}^2$ corresponding in our system to a roughly 300 fs pulse broadening through chirp. The near symmetry along both regimes of the second-order phase indicates that the pulse-duration dependence is not a group velocity dispersion issue. Aversion from the shortest pulse duration is in support of the ponderomotive model, as the ponderomotive energy is proportional to the laser pump pulse duration. The decrease in efficiency at longer pulses is due to a decrease in overall pump intensity supplied, which diminishes the ponderomotive energy. Due to the high atomic density of Ga, we expect that although tunnel ionization plays the primary role in the initialization of the plasma, cascade ionization will dominate due to the shorter mean-free paths for the electrons. This is shown in our experiment by a preference for longer pulse duration regardless of dispersion effects.

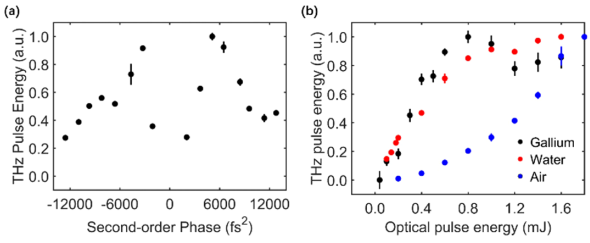

Fig. 4. (a) Normalized THz pulse energy as a function of second-order phase. (b) Normalized THz energy dependence on pump pulse energy for Ga, water, and air plasmas excited by long (>300 fs) 800 nm pulses.

Additionally, the preference for broader pulses is important for neglecting optical rectification (OR) at the surface as a major contributor to the generation mechanism. However, in our experiments we do note the appearance of a strong SHG from the LG jet, showing that the process is entirely viable.

The THz energy dependence versus pump pulse energy is shown in Fig. 4(b). Compared to experiments done in air-plasma, LG boasts a much higher conversion rate but is more prone to instability due to strong focusing. We showcase a comparison of this energy dependence measurement between the LG jet, a water jet of the same diameter (210 μm), and air plasmas. All energies were calculated under similar experimental conditions. The plotted error bars indicate the standard deviation in the measurement. THz energy for each source is individually normalized so that a general trend can be isolated. The energy yielded from the LG jet is substantially higher than that of air plasma if the same long pulse duration is used. However, air plasma boasts a higher stability than the LG jet. At pump pulse energies above 0.6 mJ, the THz energy tends toward saturation. The THz energy at this point is unexpectedly below nanojoule (nJ) level—meaning that the switch from nonlinear current generation to a plasma-based radiator significantly reduces the metal's THz yield. We believe saturation exists because in the scheme of the plasma wave, the absence of self-focusing in the material means there are no terms to balance the strong diffraction of the beam induced by plasma refraction and diffraction [14,18]. Additionally, the small length of the plasma limits the production of efficient THz. The appearance of this saturation is interesting because we know that in the non-relativistic regimes much higher efficiency can be found [1,2,19–25]. We can see this as the evidence of a change in the dominating mechanism toward CTR in the non-relativistic regime and hope to further study the turning point between our outlined mechanism and the onset of CTR.

The fluorescence and plasma emission from the LG line is also investigated by a fiber spectrometer. An uncoated and large aperture 60 mm lens is used in a 2F configuration perpendicular to the laser propagation direction to image the plasma spark onto a diffusing screen. The fiber spectrometer is placed to collect the

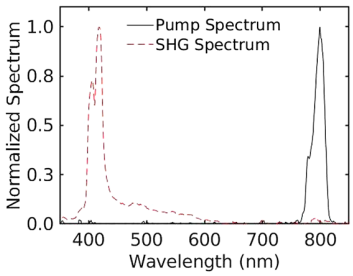

Fig. 5. Pump and second-harmonic spectra as gathered by a fiber spectrometer.

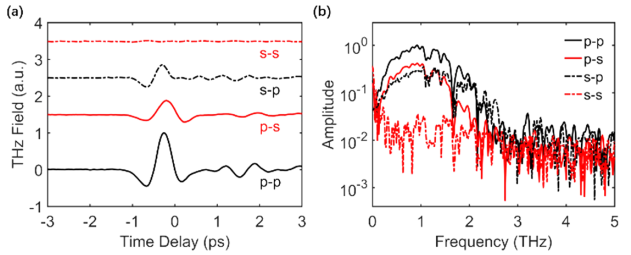

Fig. 6. (a) Normalized p- and s-polarized THz waveforms excited by the p- or s-polarized pump pulse, respectively. The first letter represents the polarization of the optical pulse, and the second letter means the polarization of the THz signal. (b) Corresponding spectra of the waveforms. THz field dependence is based on pump pulse polarization.

scatter from the diffusing screen, and an optional filter can be used to isolate frequencies higher than the second harmonic. As shown in Fig. 5, two major peaks can be found at the expected laser pump frequency and its second harmonic. We believe that this harmonic generation is due to surface nonlinearity on the metal, and we find that it is optimized at near the transform-limited pulse duration. In our manuscript we acknowledge that the presence of this radiation allows for the possibility of OR, but its dependence on the pulse duration suggest that the process is an unlikely candidate for the most efficient generation mechanism. The supercontinuum generation is broad and attributed to the nonlinear nature of the ionization process. One could surmise that the production of a harmonic of the fundamental pump frequency could lead to a photocurrent-like effect to produce highly efficient THz. However, this view is not taken in our study because of two reasons: (1) if this were the case, the directionality of the radiation would be strongly affected by the efficiency of the harmonic generated (there would exist an instance where the efficiency at zero incidence overcomes the efficiency at oblique incidences), and (2) the addition of a BBO crystal would enhance the signal to some degree. Although we do not believe that this process bears much influence on the THz yield, we believe that its appearance in the LG line experiment is interesting.

In addition to using the pulse duration argument to show that the generation from LG is different from that in the weak excitation regime, we conducted the same experiment under cylindrical lens focusing. Maintaining the same experimental parameters, we found that no THz was generated as the LG was not sufficiently ionized (the focal intensity is significantly reduced); thus, we confirm that a strong plasma is needed in this regime.

In Fig. 6, we show plots of the THz field dependence based on the pump pulse polarization. The THz beam polarization is measured by a THz wire grid polarizer, and the optical beam polarization is controlled by a half-wave plate in combination with a linear polarizer. The system is studied under four configurations: s-s, s-p, p-s, and p-p. The first and second letters represent the polarizations of the optical pulse and the THz signal, respectively. It is seen that the strongest signals are found when the pump beam is p polarized. Additionally, the THz polarization is preferentially horizontal regardless of the input pump polarization. The results show a slightly elliptical polarization that is characteristically expected in conventional plasma sources. We believe that combined with the results of translation along the x axis, there is evidence to support that the nature of the polarization is radial. Interestingly, the dependence on optical pump polarization cannot be solely attributed to the Fresnel transmission and reflection coefficients given that propagation in the LG does not occur for either wavelength. Additionally, the extinction ratio at the optical refractive index (2.09) does not match the extinction ratios observed in Fig. 6(a). The mechanism for this observation is still under investigation within our group.

In summary, we have characterized the generation mechanism and properties of a THz source based on a plasma in an LG jet. Under the non-relativistic ionizing regime, we found an optical-to-THz energy conversion efficiency of 10^{-7}. We believe the dipole and photocurrent models are applicable to the source and that the nature of the source is radial. More experiments focused on the radiation pattern and backward detection will be conducted to further understand the mechanism. We believe that studying this area will reveal important information on the behavior of plasma sources.

Funding. National Science Foundation (ECCS- 1916068); Air Force Office of Scientific Research (FA9550-18-1- 0357); Army Research Office (W911NF-17-1-0428).

Acknowledgment. The authors thank Gerrit Bruhaug for fruitful discussions regarding laser-induced plasma.

Disclosures. The authors declare no conflicts of interest.

Data Availability. Data underlying the results presented in this paper are not publicly available at this time but may be obtained from the authors upon reasonable request.

[†]These authors contributed equally to this paper.

REFERENCES

1. G. Liao, Y. Li, H. Liu, G. G. Scott, D. Neely, Y. Zhang, B. Zhu, Z. Zhang, C. Armstrong, E. Zemaityte, P. Bradford, P. G. Huggard, D. R. Rusby, P. McKenna, C. M. Brenner, N. C. Woolsey, W. Wang, Z. Sheng, and J. Zhang, "Multimillijoule coherent terahertz bursts from picosecond laser-irradiated metal foils," Proc. Natl. Acad. Sci. USA **116**, 3994–3999 (2019).
2. Y. Zeng, C. Zhou, L. Song, X. Lu, Z. Li, Y. Ding, Y. Bai, Y. Xu, Y. Leng, Y. Tian, J. Liu, R. Li, and Z. Xu, "Guiding and emission of milijoule single-cycle THz pulse from laser-driven wire-like targets," Opt. Express **28**, 15258–15267 (2020).
3. F. Kadlec, P. Kužel, and J. L. Coutaz, "Optical rectification at metal surfaces," Opt. Lett. **29**, 2674–2676 (2004).

4. F. Kadlec, P. Kužel, and J.-L. Coutaz, "Study of terahertz radiation generated by optical rectification on thin gold films," Opt. Lett. **30**, 1402–1404 (2005).
5. J.-L. Coutaz, F. Kadlec, and P. Kuzel, "Optical rectification at metal surfaces investigated in the terahertz frequency range," Proc. SPIE **6257**, 62570M (2006).
6. V. A. Mironov, I. V. Oladyshkin, E. V. Suvorov, and D. A. Fadeev, "Generation of terahertz radiation during reflection of femtosecond laser pulses from a metal surface," J. Exp. Theor. Phys. **119**, 179–195 (2014).
7. S. A. Uryupin and A. A. Frolov, "Generation of low-frequency radiation under focused laser irradiation of a conductor," Tech. Phys. **59**, 892–898 (2014).
8. E. V. Suvorov, R. A. Akhmedzhanov, D. A. Fadeev, I. E. Ilyakov, V. A. Mironov, and B. V. Shishkin, "Terahertz emission from a metallic surface induced by a femtosecond optic pulse," Opt. Lett. **37**, 2520–2522 (2012).
9. S. G. Bezhanov and S. A. Uryupin, "Free-electron mechanisms of low-frequency radiation generation on metal surfaces," Opt. Lett. **41**, 4975–4978 (2016).
10. I. V. Oladyshkin, D. A. Fadeev, and V. A. Mironov, "Thermal mechanism of laser induced THz generation from a metal surface," J. Opt. **17**, 075502 (2015).
11. P. M. Solyankin, B. V. Lakatosh, M. S. Krivokorytov, I. P. Tsygvintsev, A. S. Sinko, I. A. Kotelnikov, V. A. Makarov, J.-L. Coutaz, V. V. Medvedev, and A. P. Shkurinov, "Single free-falling droplet of liquid metal as a source of directional terahertz radiation," Phys. Rev. Appl. **14**, 034033 (2020).
12. Y. Cao, Y. E. P. Huang, and X.-C. Zhang, "Broadband terahertz wave emission from liquid metal," Appl. Phys. Lett. **117**, 041107 (2020).
13. E. Yiwen, Q. Jin, A. Tcypkin, and X. C. Zhang, "Terahertz wave generation from liquid water films via laser-induced breakdown," Appl. Phys. Lett. **113**, 181103 (2018).
14. S. Mitryukovskiy, "Coherent secondary radiation from femtosecond laser filaments," doctoral dissertation (École Polytechnique, 2014).
15. P. Sprangle, J. R. Peñano, B. Hafizi, and C. A. Kapetanakos, "Ultrashort laser pulses and electromagnetic pulse generation in air and on dielectric surfaces," Phys. Rev. E **69**, 066415 (2004).
16. S. L. Chin, *Femtosecond Laser Filamentation* (Springer, 2010), Vol. **55**.
17. K. Y. Kim, "Generation of coherent terahertz radiation in ultrafast laser-gas interactions," Phys. Plasmas **16**, 056706 (2009).
18. A. Couairon and A. Mysyrowicz, "Femtosecond filamentation in transparent media," Phys. Rep. **441**, 47–189 (2007).
19. G. Q. Liao, Y. T. Li, C. Li, H. Liu, Y. H. Zhang, W. M. Jiang, X. H. Yuan, J. Nilsen, T. Ozaki, W. M. Wang, Z. M. Sheng, D. Neely, P. McKenna, and J. Zhang, "Intense terahertz radiation from relativistic laser-plasma interactions," Plasma Phys. Controlled Fusion **59**, 014039 (2017).
20. O. Jäckel, J. Polz, S. M. Pfotenhauer, H. P. Schlenvoigt, H. Schwoerer, and M. C. Kaluza, "All-optical measurement of the hot electron sheath driving laser ion acceleration from thin foils," New J. Phys. **12**, 103027 (2010).
21. M. Ruth and M. Schollmeier, "Ion acceleration—target normal sheath acceleration (CERN Yellow Reports)," in *CAS-CERN Accelerator School: Plasma Wake Acceleration*, Geneva, Switzerland, 2016, Vol. **001**, pp. 231–270.
22. S. Zhang, J. Yu, Y. Shou, Z. Gong, D. Li, Y. Geng, W. Wang, X. Yan, and C. Lin, "Terahertz radiation enhanced by target ablation during the interaction of high intensity laser pulse and micron-thickness metal foil," Phys. Plasmas **27**, 023101 (2020).
23. A. Debayle, F. Mollica, B. Vauzour, Y. Wan, A. Flacco, V. Malka, X. Davoine, and L. Gremillet, "Electron heating by intense short-pulse lasers propagating through near-critical plasmas," New J. Phys. **19**, 123013 (2017).
24. S. Herzer, A. Woldegeorgis, J. Polz, A. Reinhard, M. Almassarani, B. Beleites, F. Ronneberger, R. Grosse, G. G. Paulus, U. Hübner, T. May, and A. Gopal, "An investigation on THz yield from laser-produced solid density plasmas at relativistic laser intensities," New J. Phys. **20**, 063019 (2018).
25. A. V. Arefiev, V. N. Khudik, A. P. L. Robinson, G. Shvets, L. Willingale, and M. Schollmeier, "Beyond the ponderomotive limit: direct laser acceleration of relativistic electrons in sub-critical plasmas," Phys. Plasmas **23**, 056704 (2016).